Journal of the European Ceramic Society **18** (1998) 261–268

PII: S0955-2219(97)00112-X
0955-2219/98/$19.00 + 0.00

Processing of Mullite Ceramic from Alkoxide-derived Silica and Colloidal Alumina with Ultra-high Cold Isostatic Pressing

Yong Ick Cho,[a]* Hidehiro Kamiya,[a] Yoshio Suzuki,[a] Masayuki Horio[a] and Hisao Suzuki[b]

[a]Graduate School of Bio-Applications and Systems Engineering, Tokyo University of Agriculture and Technology, Koganei, Tokyo, 184 Japan
[b]Shizuoka University, Hamamatsu, Shizuoka, 432 Japan

(Received 4 March 1997; accepted 30 May 1997)

Abstract

Ultra-fine mullite precursor powders were prepared from the uniform mixtures of ultra-fine γ–Al_2O_3 and alkoxide-derived SiO_2 powders. Two kinds of mixing methods—ball milling and stirring—were used to change the level of mixing. The ball milling method attained the more uniform mixing state to form single phase mullite after the calcination of mixed powder at 1300°C. Green compacts of the calcined precursor powders were consolidated by ultra-high cold isostatic pressing up to 1 GPa. Since ultra-high isostatic pressure offers the close packing structure in the green compacts, the maximum relative density of the green compacts reached about 60% of theoretical in which the inter-aggregate pore was collapsed to reduced the pore size below 6 nm. These closely and uniformly packed green compacts could be sintered almost full density of a stoichiometric mullite ceramic without glassy and other crystalline phase. Maximum density of the compacts reached more than 96% of theoretical by the pressureless sintering even below liquid formation temperature. As a result, dense mullite ceramic with a stoichiometric composition and fine microstructure composed of grains below 0·5 μm could be sintered at relatively low temperatures. © *1997 Elsevier Science Limited.*

1 Introduction

Highly pure and stoichiometric mullite ceramic ($3Al_2O_3{\cdot}2SiO_2$) has intrinsic high creep resistance, chemical and thermal stability and high strength at high temperatures.[1,2] However, the densification of mullite ceramics proceeds above liquid formation temperature (≥1587 ± '10°C), resulting in the residual glassy phase after sintering. This leads to the reduced mechanical properties at high temperature and credibility of ceramics. Several researchers have synthesized mullite precursor powders from different available SiO_2 and Al_2O_3 source materials.

The polymeric sol–gel process or colloidal process for mullite precursor powders have been promoting the need for high purity and homogeneity at relatively low temperature sintering. Polymeric process,[3–8] allow the molecular design of the precursors by controlling the hydrolysis and condensation of aluminum and silicon alkoxide. Rapid mullitization of these molecular designed powders is possible below 1000°C; however, densification is very difficult without high temperature sintering (~1700°C) or hot-pressing, because rapid crystallization and hard aggregation of precursor powders hinders the full densification even at elevated temperature. In contrast, densification of the colloidal mullite precursor[9–24] from γ-Al_2O_3 or boehmite and silica-sol proceeds by a viscous sintering mechanism of amorphous silica.[23,25–27] Sacks *et al.* reported the transient viscous sintering of composite powders prepared from silica-coated α-Al_2O_3.[27] However, the viscous flow sintering was likely to produce coarse grain structure, resulting in the residual unreactive α-Al_2O_3 and glass phase even by the relatively high temperature sintering (~1600°C),[11,12,19,28] although a heat treatment time-temperature profile was designed[23] for optimizing the densification.

On the other hand, the effect of pressure on the hydrates powder densification has been previously

*To whom correspondence should be addressed.

studied.[29] However, the maximum pressures in this paper were limited to 20 MPa. We have demonstrated in previous papers that the molecular designed ultra-fine mullite precursor with a stoichiometric composition could be prepared[30] and consolidated into a close packing structure up to about 70% of theoretical density by using ultra-high pressure cold isostatic press up to 1 GPa.[31,32] In this process, almost fully densified stoichiometric mullite ceramic with a very fine microstructure can be sintered below liquid formation temperature of 1500°C. Close packing of ultra-fine powder compacts allowed the almost full densification of a stoichiometric mullite at relatively low-temperature sintering.

In this paper, a better mixing process to form uniform hetero-coagulation between ultra-fine colloidal γ-Al_2O_3 and alkoxide-derived SiO_2 powder was developed to prepare a dense stoichiometric mullite ceramic with no inclusion of other phase. The uniformly and stoichiometric hetero-coagulated colloidal precursor powders were consolidated into highly dense green compact by ultra-high pressure cold isostatic press (up to 1 GPa). The effect of isostatic pressure, primary particle size and the level of mixing on the densification behavior during sintering and the microstructure of the sintered bodies are discussed.

2 Experimental Procedure

2.1 Preparation of mullite precursor powders

Spherical ultra-fine SiO_2 powders with a narrow size distribution were prepared by the controlled hydrolysis and condensation of metal alkoxide.[31] Under the constant stirring and temperature, tetraethyl orthosilicate (TEOS) was titrated into a mixed ethanol and ammonium hydroxide solution with different concentration, and mixed for 72 h to complete the hydrolysis and following condensation reaction of TEOS. Then, excess water (about 110 ml) was added and mixed for 72 h to form a stable electrical double layer on the particles, leading to the uniform dispersion of the resultant sol. Commercial ultra-fine γ-Al_2O_3 powder (TM-100 or TM-300, Taimei Chemical, Ltd., Nagano, Japan; specific surface area was 134 and 290 $m^2 g^{-1}$, respectively) was added into the alkoxide-derived SiO_2 sol to mix under the constant stirring or by the ball milling for 24 h. The typical amount of γ-Al_2O_3 powder, TEOS, ethanol, distilled water and Conc. ammonium hydroxide (29%) used in the experiment were 10 g, 30, 370, 32, 2·9 ml, respectively. The concentration of TEOS and the hydrolysis water were fixed at 0·3 and 4·5 $mol l^{-1}$, respectively. The primary particle diameter of SiO_2 sol were controlled in the range from 10 nm to 60 nm by changing the concentration of ammonium hydroxide. The total amount of the sol was about 450 ml, and the molecular ratio of Al to Si was fixed at 3:2, corresponding to a stoichiometric mullite.

Granules of mullite precursor powders were prepared by spray-drying the mixed sols of alkoxide-derived SiO_2 and γ-Al_2O_3 at 170°C. Spray-dried granules were calcined for 24 h at 80°C to remove the residual water on powder surface. The size distribution of aggregates in suspension after mixing was determined by a centrifugal sedimentation method. Specific surface area, S_w of the calcined powder was measured by nitrogen gas absorption method (single-point BET method). Estimated mean particle diameter d_B (nm), was calculated by the following equation and specific surface area, S_w:

$$d_B = 6000/(S_W \cdot \rho_T)$$

where ρ_T is the true density of the SiO_2 powder, γ-Al_2O_3 powder or their mixtures. The unit for surface area, density, and diameter used are $m^2 g^{-1}$, $g cm^{-3}$, and nm. The estimated mean diameters of γ-Al_2O_3 (S_w = 134 and 290 $m^2 g^{-1}$) were 14 and 7 nm, respectively. The size of SiO_2 particles, d_{EM}, was determined by TEM observation. Thermal gravimetric analysis (TG) and differential thermal analysis (DTA) were carried out in flowing air (70 ml min^{-1}) at a heating rate of 10°C min^{-1}. After the calcination up to 1300°C, crystalline phases of the calcined mullite precursor powders were identified by the powder X-ray diffraction technique.

2.2 High-pressure isostatic pressing of mullite precursor powder

Calcined granules were packed into a cylindrical cell with a diameter of 2 cm and uniaxially pre-pressed at 5·5 MPa for 3 min. Then, the green compacts were isostatically pressed in the range from 5·5 MPa to 1 GPa for 3 min (Model MCT-100, Mitsubishi Heavy Industries, Tokyo). The green density and pore size distribution of the green compacts were measured by mercury porosimetry. Complete dehydration and dehydroxylation of each precursor powder required temperature higher than 1000°C as determined by TG analysis. The mean weight loss of each precursor powder was 9·6 wt% (SiO_2 = 10 nm), 8·6wt% (SiO_2 = 30 nm) and 8·9 wt% (SiO_2 = 60 nm) at 1000°C. Based on these results, the weight of the green compacts was obtained by subtracting the amount of adsorbed water and hydroxyl on precursor powders. The

apparent volume of the green compacts as measured on condition that the pressure applied on mercury was sufficiently low value (about 6·8 kPa) not to detect the pore at the surface of compacts.

2.3 Sintering behavior of green compacts

Sintering was carried out in an electric furnace at different temperatures ranging from 1400 to 1600°C for 2 h at a heating rate of 200°C h^{-1}. Bulk density of the sintered bodies was measured by an Archimedes method using distilled water. If the relative density of the sintered bodies was lower than 90% of theoretical, bulk density was determined by mercury porosimetry. Microstructure observations were made on polished and thermal etched samples with SEM.

Densification of the green compacts was also examined by a dilatometer (Model TAS-100, Rigaku Corporation, Tokyo). The change in the bulk density of each sample during sintering was determined from the weight and the liner shrinkage.

3 Results and Discussion

3.1 Characterization of precursor powders prepared by different mixing methods

Figure 1 shows the size distribution of the agglomerated colloidally mixed powders. Mean primary particle diameters of raw powders were 10 nm for alkoxide-derived SiO_2 and 14 nm for γ-Al_2O_3, respectively. The estimated aggregate size in suspension depended on the mixing methods. Raw γ-Al_2O_3 powders formed large aggregates within their suspension, estimated mean diameter was about 2 μm. In the case of the stirring mixing, the aggregate size in suspension did not change after mixing and was independent of the mixing time. On the contrary, aggregate structure was effectively collapsed during ball-milling to reduce the mean diameter of the aggregates in suspension with increasing milling time. The mean diameter of the raw powder mixture of 2 μm was reduced to 0·15 μm by the 24-h ball-milling.

Aggregate structure in suspensions affected the structure of spray-dried granules. Figure 2 shows typical examples of pore size distributions in the packed beds of spray dried granules prepared from suspension with different primary particle sizes and mixing methods. The mean diameter of the SiO_2 particles used were 10 nm and 60 nm, while keeping the γ-Al_2O_3 size constant. Although the raw powders had broad dispersion of the aggregate size, the pore size distribution in the packed bed of granules prepared by ball-milling process showed narrower peak at smaller pore size than that of the granules prepared by the stirring method. In the case of the stirring method, relatively larger pores more than 100 nm in diameter existed in the granules. If the mean diameter of the SiO_2 particle was larger than

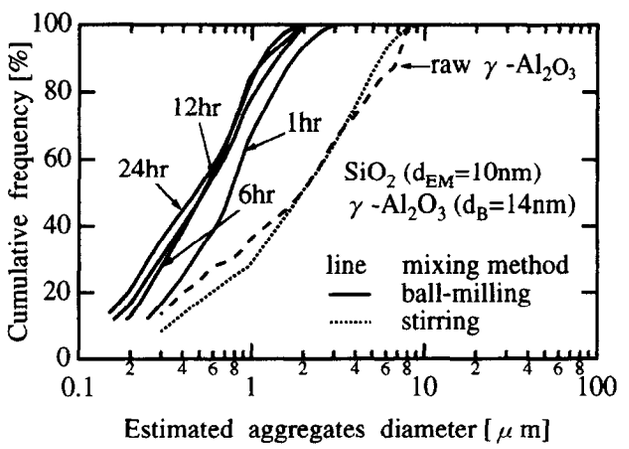

Fig. 1. Effect of mixing method, ball-milling or stirring method, and mixing time on aggregate size distribution in suspension determined by a centrifugal sedimentation method. Raw powders used were ultra-fine γ-Al_2O_3 (d_B = 14 nm) and SiO_2 (dEM = 10 nm) powders.

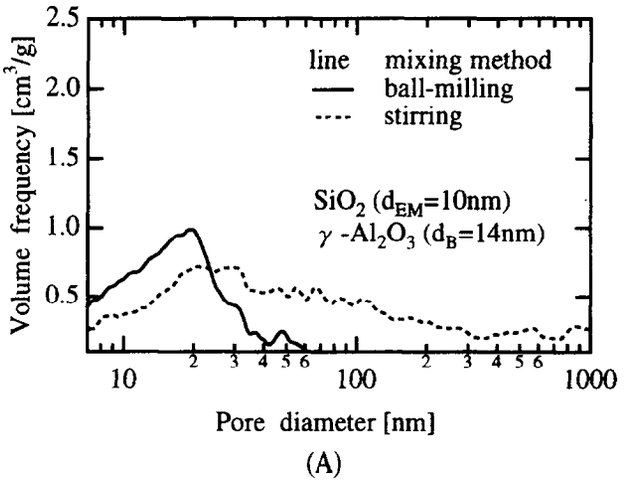

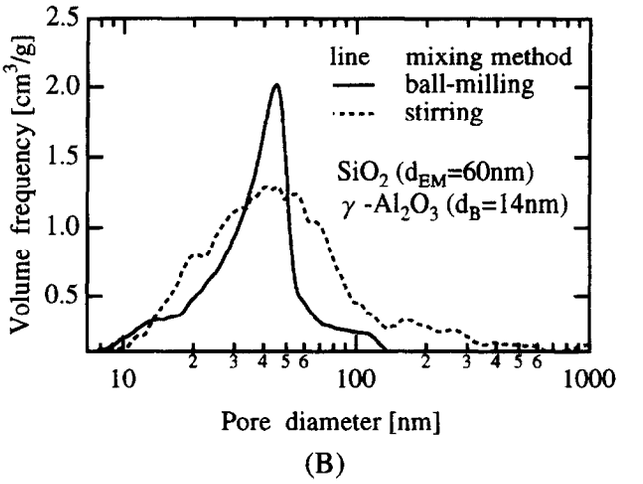

Fig. 2. Effect of mixing method and particle size on pore size distribution in packed bed of spray-dried granules prepared from hetero-coagulation precursor powders with different SiO_2 particle diameters.

60 nm in diameter, SiO_2 particles were well dispersed in suspension, however, since ultra-fine SiO_2 powder of 10 nm in diameter tended to form larger aggregates than the primary particle size and showed wide pore size distribution.

The level of mixing also affected on the crystalline phases in the precursor powders after calcination. Figure 3 shows the X-ray diffraction patterns of the colloidally mixed powders calcined at 1300°C. Calcined powders mixed by a stirring method crystallized into mixtures of α-Al_2O_3, cristobalite and mullite at 1300°C [Fig. 3(A)]. A small amount of additional phases of α-Al_2O_3 and cristobalite was retained in this powder, even though the calcining temperature was elevated to 1600°C. Because a stirring method could not collapse the aggregate structure to form the uniform mixture of each colloidal powder, additional phases including glassy phase remained in the calcined powders. The same results had been reported in many papers concerning colloidal process for mullite ceramics.[23] On the contrary, only the mullite phase was identified in the calcined powders mixed by the ball-milling process. This showed that ball-milling process collapse the aggregate structure in the raw powders to achieve uniform hetero-coagulation between γ-Al_2O_3 and SiO_2.

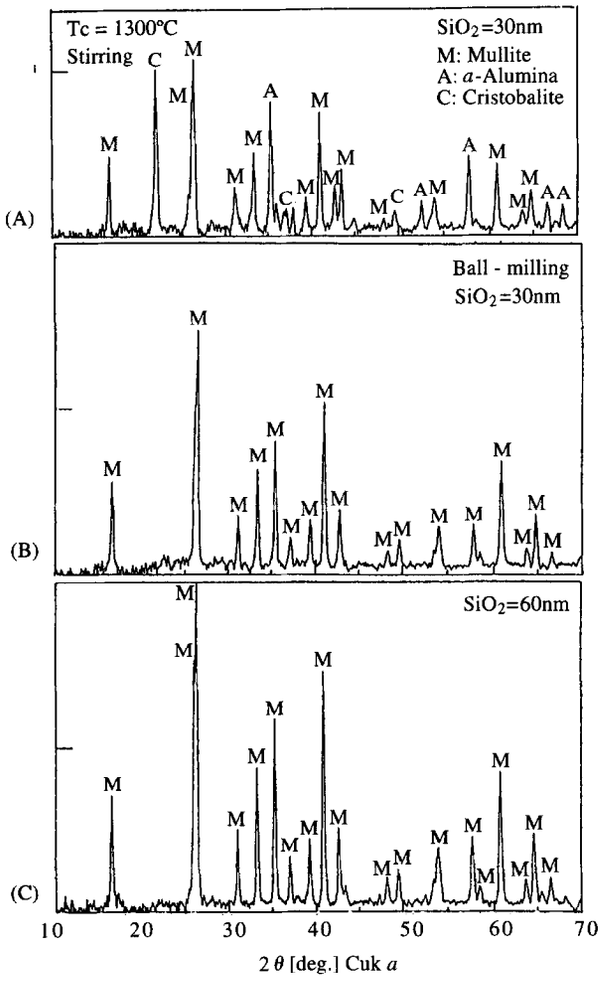

Fig. 3. XRD analysis of various raw powders calcined at 1300°C. Mixing method was (A) stirring, and (B) and (C) ball milling method. Estimated particle diameters of SiO_2 powders were (A) 30 nm, (B) 30 nm, (C) 60 nm, respectively, and γ-Al_2O_3 was fixed at 14 nm in diameter.

3.2 Forming behavior of green compacts under ultra-high cold isostatic pressing

Ultra-fine powders can not stuff into close packing structure because of their hard and coarse agglomerates. Ultra-high isostatic pressure is expected to collapse the hard and coarse structure of the agglomerates and rearrange the particles to form the close packing structure. Figure 4 shows the consolidation behavior of the green compacts of the colloidal precursor powders with different diameter and mixing methods. The relative density of the powder compacts were lower than 30% of theoretical when the isostatic pressure for forming was lower than 0·01 GPa. However, the relative density increased with increasing isostatic pressure, p_c, and reached about 60% in all samples if the $p_c = 1$ GPa. The primary particle diameter and mixing method slightly affected the green density.

Figure 5 shows typical examples of the pore size distributions in the green compacts after isostatic pressing at different pressures. Mean primary particle diameters are 30 nm for SiO_2 and 14 nm for Al_2O_3 colloidal particles. In the case of low isostatic pressure ($p_c = 5$ MPa), bimodal pore size distribution was found and the larger pores decreased

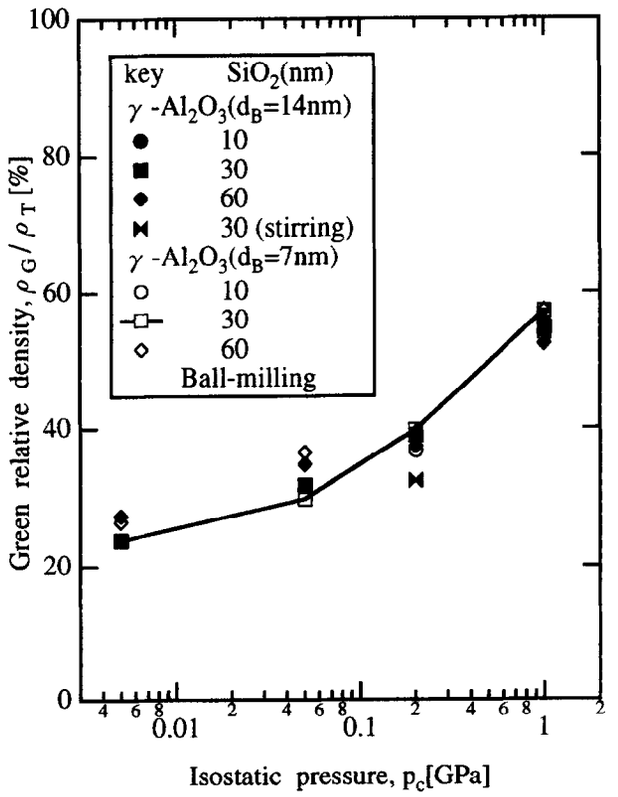

Fig. 4. Relationship between relative density of green compacts with different raw powders and cold isostatic pressures.

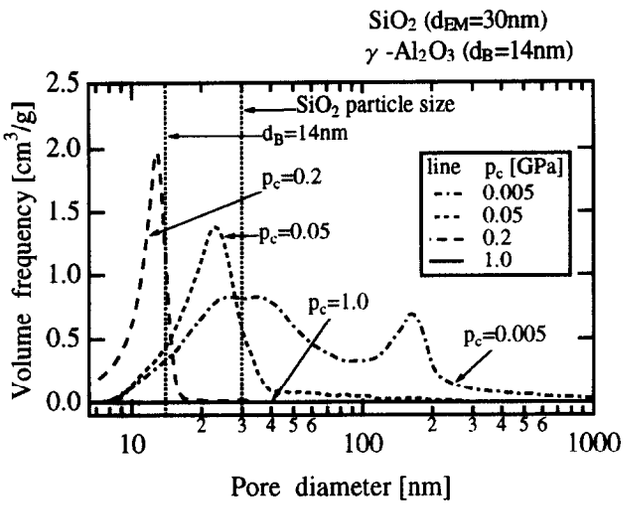

Fig. 5. Examples of pore size distribution in green compacts after cold isostatic pressing with different pressures. Mean diameter of γ-Al_2O_3 and SiO_2 were 14 nm ($S_w = 290\,m^2\,g^{-1}$), and 30 nm, respectively.

with increasing isostatic pressures. The pores larger than the estimated primary particle diameter, 14 nm, disappeared at 0·2 GPa. Furthermore,if the isostatic pressure was applied at 1 GPa, no pore was detected by the mercury porosimetry. This showed the inter-aggregate pore was completely collapsed and the primary particles were rearranged to form close packing structure after ultra-high isostatic pressing.

3.3 Sintered density of green compacts

Figure 6 shows the difference between mixing methods for the preparation of raw powders on the dilatometry behavior of the powder compacts during heating. Samples were consolidated by the ultra-high pressure (1 GPa). Typical densification of both samples occurred between 1100 and 1250°C. Above 1300°C, raw powders crystallized into mullite phase, resulting in the decrease of the shrinking rate. Because the viscous sintering by the amorphous silica was pronounced in the region above 1100°C, densification of green compacts was accelerated in the range from 1100 to 1250°C. However, the difference between the two dilatometric trace, ball milling and stirring, is very small.

The effect of the level of mixing and other additional effects of ball milling, which are local high pressure or heating during mixing, on the densification were negligible. Densification of colloidal precursor powders were mainly preceded by the viscous flow sintering mechanism of the amorphous silica and the reaction between amorphous silica and γ-Al_2O_3 to form mullite. The formation of the excess glassy phase during sintering did not promote the densification of compacts. Inhomogeous hetero-coagulation of the precursor powders prepared by a stirring method resulted in the additional phase of α-Al_2O_3 and cristobalite at 1300°C [Fig. 3(A)] and the grain growth in the resultant mullite ceramics. The formation of the additional phases would not only reduce the mechanical properties of the resultant ceramic but also hinder the viscous sintering.

Figure 7 shows the effect of isostatic pressure on the bulk density of the sintered bodies as a function of the sintering temperature. Mean diameters of Al_2O_3 and SiO_2 were 14 nm and 30 nm, respectively. The bulk density increased with increasing isostatic pressure. The relative bulk densities at 1450°C were (based on mullite $3{\cdot}17\,g\,cm^{-3}$) 71% for 0·05GPa, 80% for 0·2 GPa and 97% for 1 GPa. In addition, the temperatures at which the density increase leveled off decreased with increasing isostatic pressure. This may be due to the difference in the initial density or diffusion path length to complete mullitization. In this case, the density was

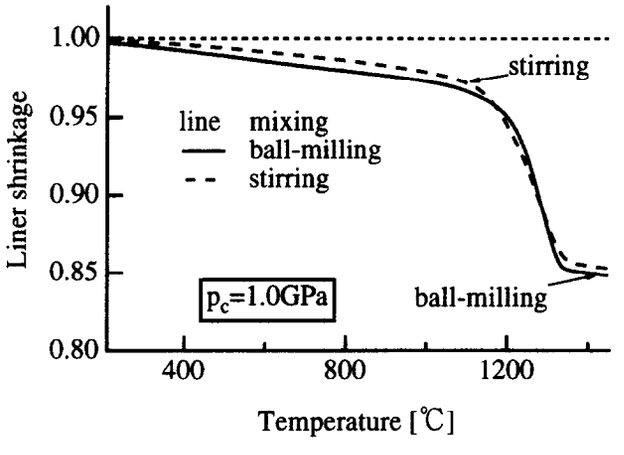

Fig. 6. Effect of the uniformity of hetero-coagulated of precursor powders on diametric behavior of green compacts consolidated by ultra-high isostatic pressure (1 GPa). The heating rate was at $20°C\,min^{-1}$.

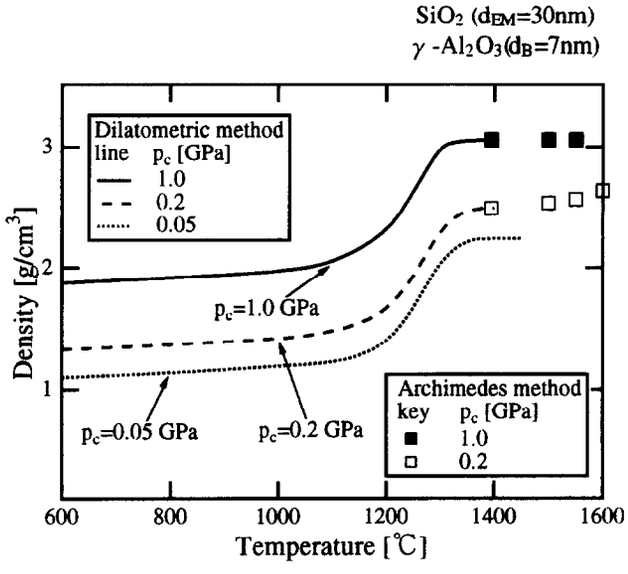

Fig. 7. Effect of cold isostatic pressure on densification behavior during sintering.

determined by an Archimedes method at above 1400°C and by dilatometric method below 1400°C. Therefore, ultra-high isostatic pressure would achieve not only the closed packing of primary particle, to form mullite phase at lower temperatures but also promote the grain growth at low temperatures, leading to the low-temperature sintering.

Effect of primary particle size of the raw γ-Al_2O_3 powders on the sintered density was also shown in Fig. 8. Precursor powders were prepared by a ball-milling method. The distinguishing effect of the primary particle size of γ-Al_2O_3 powders was observed on the densification behavior. The higher final density and lower mullitization temperature were achieved in the case of ultra-fine γ-Al_2O_3 powders (7 nm). On the other hand, SiO_2 particle size slightly affected on the densification behavior. This may be ascribed to the sintering mechanism. Since amorphous silica particles were deformed by the ultra-high isostatic pressure, and attributed to the viscous flow at relatively low temperatures, particle size of raw SiO_2 powders did not have an effect.

3.4 Microstructure

Figure 9 shows SEM micrographs of polished and thermally etched samples sintered at 1400°C for 2h after ultra-high cold isostatic pressure of 1 GPa. Mean estimated particle diameters of SiO_2 used were 30 nm and that of the γ-Al_2O_3 powders were (A) 14 nm and (B) 7 nm. Relative densities estimated by Archimedes methods were (A) 90% and (B) 96% of theoretical. The microstructure of both sintered samples showed almost pore-free and fine microstructure. Primary particle size of γ-Al_2O_3 slightly influenced on the grain size and distribution of the grain sizes in each sample. The size distribution ranged (A) 0·1~1·0 μm and (B) 0·1~0·5 μm. XRD analysis [Fig. 3(B)] showed that mullitization completed at 1300°C in the case of colloidally mixed powder by ball milling. Microstructure of mullite ceramics sintered at 1600°C was shown in Fig. 10. The preparation condition was same as that of Fig. 9(A). Judging from Fig. 10, almost all grain was less than 1 μm in diameter.

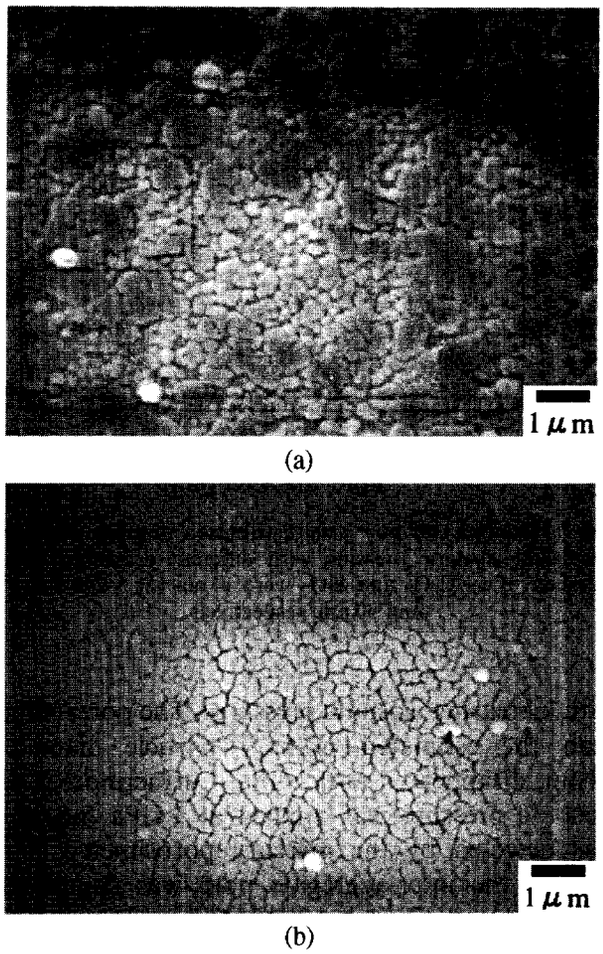

Fig. 9. SEM micrographs of polished and thermally etched samples sintered at 1400°C for 2 h. Precursor powders were prepared by ball-milling method. Estimated mean particle diameter was 30 nm for SiO_2, and γ-Al_2O_3 particles used were (A) 14 nm, (B) 7 nm. Isostatic pressure was 1 GPa.

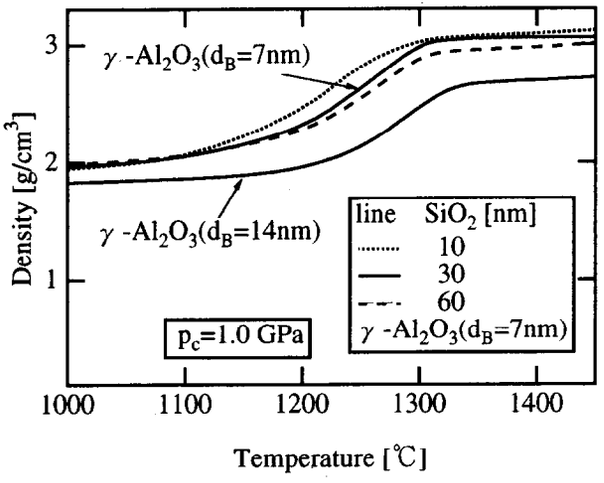

Fig. 8. Effect of primary particle diameter of γ-Al_2O_3 and SiO_2 powders on densification behavior.

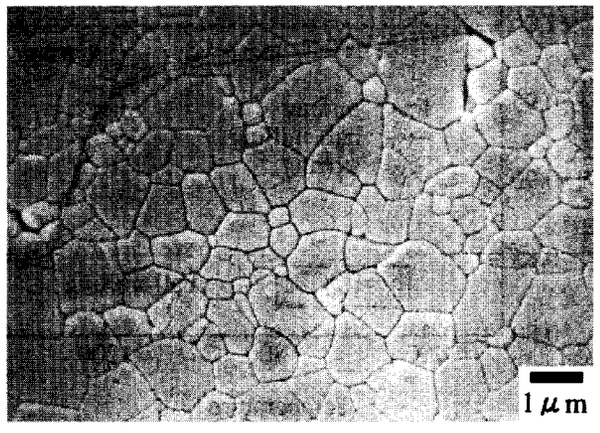

Fig. 10. SEM micrographs of polished and thermally etched sample sintered at 1600°C for 2 h. Precursor powder was prepared by the ball milling method. Mean diameter was 14 nm for γ-Al_2O_3 powder and 30 nm for SiO_2.

Fig. 11. SEM micrographs of polished and thermally etched sample sintered at 1600°C for 2 h. Precursor powder was prepared by stirring method. Mean diameter was 14 nm for γ-Al_2O_3 and 30 nm for SiO_2.

The microstructure of the sintered sample prepared from inhomogeneous precursor powders mixed by a stirring method is shown in Fig. 11. Raw powders were same as that of the Fig. 10. In this case, cristobalite and α-Al_2O_3 phase remained in each sample [Fig. 3(A)] and the grain size was larger than that of the samples prepared from homogeneous hetero-coagulation precursors (Fig. 10). Inhomogeneous hetero-coagulation resulted in the additional phase formation and anomalous grain growth.

4 Conclusion

Colloidal precursor powders for a stoichiometric mullite ceramic were prepared from ultra fine γ-Al_2O_3 and alkoxide-derived SiO_2 powder with different diameters and by using different mixing methods. Each powder was spray-dried and consolidated with ultra-high cold isostatic pressing up to 1 GPa, to attain low-temperature sintering. The mixing method influenced on the uniformity of the resulting precursor powders. Stirring method resulted in the inhomogeous mixing to form additional phases of α-Al_2O_3, and cristobalite in the powders calcined at 1300°C. On the contrary, ball-milling method offered the uniform mixing and lower mullitization temperatures without any other phase formation after calcination at 1300°C. Ultra-high isostatic pressure up to 1 GPa led to a dense packing structure of the green compacts to achieve the maximum green density of about 60% of theoretical. Ultra-high isostatic pressure was completely collapsed inter-aggregate pore in the green compact to reduce the pore size below 6 nm.

As a result, these densely packed green compacts sintered into almost full density more than 95% of theoretical, at above 1300°C. Furthermore, the low-temperature sintering process based on the hetero-coagulation of the raw SiO_2 and Al_2O_3 powders led to the fine grain size of the resulting mullite ceramic.

References

1. Dokko, P. C., Pask, J. A. and Mazdiyasni, K. S., High-temperature mechanical properties of mullite under compression. *J. Am. Ceram. Soc.*, 1977, **60**, 150–155.
2. Lessing, P. A., Gordon, R. S. and Mazdiyasni, K. S., Creep of polycrystalline mullite. *J. Am. Ceram. Soc.*, 1975, **58**, 149.
3. Okada, K. and Otsuka, N., Characterization of the spinel phase from SiO_2–Al_2O_3 xerogels and the formation process of mullite. *J. Am. Ceram. Soc.*, 1986, **69**, 652–656.
4. Yoldas, B. E., Microstructure of monolithic materials formed by heat treatment of chemically polymerized precursors in the Al_2O_3–SiO_2 binary. *Am. Ceram. Soc. Bull.*, 1980, **59**, 479–483.
5. Pask, J. A., Zhang, X. W., Tomsia, A. P. and Yoldas, B. E., Effect of sol–gel mixing on mullite microstructure and phase equilibria in the α-Al_2O_3–SiO_2 system. *J. Am. Ceram. Soc.*, 1987, **70**, 704–707.
6. Yoldas, B. E. and Partlow, D. P., Formation of mullite and other alumina-based ceramics via hydrolytic polycondensation of alkoxides and resultant ultra- and microstructure effects. *J. Mater. Sci.*, 1988, **23**, 1895–1900.
7. Li, D. X. and Thomson, W. J., Mullite formation kinetics of a single-phase gel. *J. Am. Ceram. Soc.*, 1990, **73**, 964–969.
8. Chakravorty, A. K. and Ghosh, D. K., Synthesis and 980°C phase development of some mullite gels. *J. Am. Ceram. Soc.*, 1988, **71**, 978–987.
9. Wei, W. C. and Halloran, J. W., Transformation kinetics of diphasic aluminosilicate gels. *J. Am. Ceram. Soc.*, 1988, **71**, 581–587.
10. Huling, J. C. and Messing, G. L., Hybrid gels for homoepitactic nucleation of mullite. *J. Am. Ceram. Soc.*, 1989, **72**, 1725–1729.
11. Li, D. X. and Thomson, W. J., Kinetic mechanisms for mullite formation from sol–gel precursors. *J. Mater. Res.*, 1990, **5**, 1963–1969.
12. Fahrenholtz, W. G., Smith, D. M. and Cesarano III, J., Effect of precursor particle size on the densification and crystallization behavior of mullite. *J. Am. Ceram. Soc.*, 1993, **76**, 433–437.
13. Hoffman, D. W., Roy, R. and Komarneni, S., Diphasic xerogels, a new class of materials: phases in the system Al_2O_3–SiO_2. *J. Am. Ceram. Soc.*, 1984, **67**, 468–471.
14. Komarneni, S., Suwa, Y. and Roy, R., Application of compositionally diphasic xerogels for enhanced densification the system Al_2O_3–SiO_2. *J. Am. Ceram. Soc.*, 1986, **69**, C155–C156.
15. Rahaman, M. N., DeJonghe, L. C., Shinde, S. and Tewari, P. H., Sintering and microstructure of mullite aerogels. *J. Am. Ceram. Soc.*, 1987, **71**, C348–C351.
16. Aksay, I. A., Dabbs, D. and Sarikaya, M., Mullite for structural, electronic, and optical applications. *J. Am. Ceram. Soc.*, 1991, **74**, 2343–2358.
17. Okada, K., Otsuka, N. and Somiya, S., Recent mullitization studies in Japan: a review. *Am. Ceram. Soc. Bull.*, 1991, **70**, 2414–2418.
18. Klaussen, G., Fischman, G. S. and Laughner, J. L., Microstructural evolution of sol–gel mullite. *Ceram. Eng. Sci. Proc.*, 1990, **11**, 1087–1093.
19. Ismail, M. G. M. U., Nakai, Z. and Somiya, S., Microstructure and mechanical properties of mullite prepared by the sol–gel method. *J. Am. Ceram. Soc.*, 1987, **70**, C7–C8.
20. Sundaresan, S. and Aksay, I. A., Mullitization of diphasic aluminosilicate gels. *J. Am. Ceram. Soc.*, 1991, **74**, 2388–2392.

21. Rahaman, M. N., Jonghe, L. C. D., Shinde, S. L. and Tewari, P. H., Sintering and microstructure of mullite aerogels. *J. Am. Ceram. Soc.*, 1988, **71**, C338–C341.
22. Li, D. X. and Thomson, W. J., Mullite formation from nonstoichiometric diphasic precursors. *J. Am. Ceram. Soc.*, 1991, **74**, 2382–2387.
23. Fahrenholtz, W. G. and Smith, D. M., Densification and microstructure of sodium-doped colloidal mullite. *J. Am. Ceram. Soc.*, 1994, **77**, 1377–1380.
24. Prochazka, S. and Klug, F. J., Infrared-transparent mullite ceramic. *J. Am. Ceram. Soc.*, 1983, **66**, 874–880.
25. Wang, J. G., Ponton, C. B. and Marquis, P. M., Effects of green density on crystallization and mullitization in the transiently sintered mullite. *J. Am. Ceram. Soc.*, 1992, **75**, 3457–3461.
26. Rahaman, M. N. and De Jonghe, L. C., Effect of rigid inclusions on the sintering of glass powder compacts. *J. Am. Ceram. Soc.*, 1987, **70**, C348–C351.
27. Sacks, M. D., Bozkurt, N. and Scheiffele, G. W., Fabrication of mullite and mullite–matrix composites by transient viscous sintering of composite powders. *J. Am. Ceram. Soc.*, 1991, **74**, 2428–2437.
28. Mroz, T. J. and Laughner, J. W., Microstructures of mullite sintered from seeded sol–gels. *J. Am. Ceram. Soc.*, 1989, **72**, 508–509.
29. Child, P. E., Howe, A. T. and Shilton, M. G., Studies of layered uranium (VI) compounds. V. Mechanisms of densification of hydrogen uranyl phosphate tetrahydrate (HUP): pressure-induced planar glide and solution phase sintering. *J. Solid State Chem.*, 1980, **34**, 341–346.
30. Suzuki, H., Tomokiyo, Y., Suyama, Y. and Sato, H., Preparation of ultra-fine mullite powder from metal alkoxide. *J. Ceram. Soc. Jpn.*, 1988, **96**, 67–73.
31. Kamiya, H., Suzuki, H., Ichikawa, T. and Jimbo, G., Ultra-high pressure cold isostatic pressing. *Ceram. Eng. and Sci. Pro.*, 1992, **13**, 563–570.
32. Kamiya, H., Suzuki, H., Kato, D. and Jimbo, G., Densification of alkoxide-derived fine silica powder compact by ultra-high-pressure cold isostatic pressing. *J. Am. Ceram. Soc.*, 1993, **76**, 54–64.